

Species-Specific Uptake of Arsenic on Confined Metastable 2-Line Ferrihydrite: A Combined Raman-X-Ray Photoelectron Spectroscopy Investigation of the Adsorption Mechanism

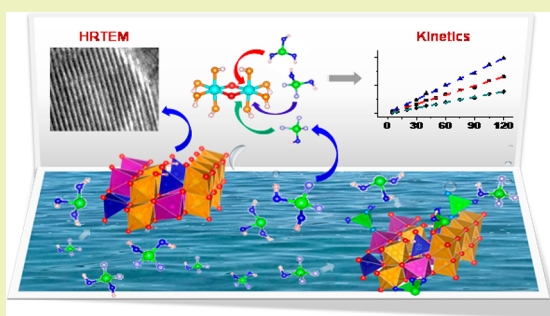
Chennu Sudhakar, Avula Anil Kumar,¹ Radha Gobinda Bhui, Soujit Sen Gupta, Ganapati Natarajan, and Thalappil Pradeep*²

DST Unit of Nanoscience (DST UNS) and Thematic Unit of Excellence (TUE), Department of Chemistry, Indian Institute of Technology Madras, Chennai 600036, India

S Supporting Information

ABSTRACT: The present study is targeted toward understanding the interaction between important and technologically relevant polymorphs of iron oxides/oxyhydroxides with arsenic species at neutral pH. The existence of various arsenic (As) species in solution was verified by Raman measurements. Their species-dependent adsorption on the affordable arsenic removal media, confined metastable 2-line ferrihydrite (CM2LF) was investigated. The results were compared with common adsorption media, hematite (α -Fe₂O₃) and magnetite (Fe₃O₄). X-ray photoelectron spectroscopy was used to investigate the changes in the core levels of Fe 2p and As 3d resulting from the uptake of arsenic species. Binding of various As species with CM2LF was confirmed by FTIR studies. Raman adsorption data were found to fit a pseudo-second-order model. Results of this study show the synthesized nanocomposite of CM2LF to be very effective for the removal of As(III) and As(V) species in comparison to various materials at neutral pH. A model for the adsorption of As(III) and As(V) species in water on a ferrihydrite particle was developed. This accounted for the large uptake capacity.

KEYWORDS: Arsenic species, Uptake capacity, CM2LF, Hematite, Magnetite, Adsorption mechanism



INTRODUCTION

Arsenic is one of the major contaminants in drinking water in many parts of the world. Various parts of India, Bangladesh, Cambodia, South Africa, Argentina, United States, and other countries have arsenic in the groundwater to an extent more than the permissible limit, namely 10 $\mu\text{g L}^{-1}$ (10 ppb) prescribed by the World Health Organization (WHO).^{1,2} Arsenic and its associated problems are still a great threat to human health, although arsenic in water was first reported by Benjamin Martin way back in 1759.³ Arsenic occurs in natural waters as either arsenite (As(III)) or arsenate (As(V)).⁴ Both forms of arsenic have strong affinity for iron oxide/oxyhydroxide surfaces near neutral pH.^{5,6} The speciation of arsenic is an important aspect for understanding its mobility, bioavailability, and toxicity in groundwater.⁷ A comprehensive solution for arsenic contamination was not evident as efforts made previously have faced various challenges. Arsenic in the environment has been addressed in various ways in terms of technology, and all of them have certain limitations.⁸

In this context, there is a need to explore the use of nanomaterials for arsenic mitigation due to their large surface area and enhanced surface reactivity. In the past decade, various nanostructured composites have been used to remove arsenic from water, namely, graphene oxide–MnFe₂O₄ nano-hybrids,⁹ Fe–Cu binary oxides,¹⁰ nanocrystalline TiO₂,^{3,11,12}

superparamagnetic Mg_{0.27}Fe_{2.5}O₄,¹³ GO–ZrO(OH)₂ nanocomposites,¹⁴ GNP/Fe–Mg oxide,¹⁵ etc. Recently, researchers have looked at several bioadsorbents like Eichhornia crassipes which are locally available. Powders of the roots of Eichhornia crassipes, possessing multiple functional groups (–OH, –NH₂, and –COOH) on the surface, were used for the potential removal of arsenic species from wastewater.¹⁶

However, to know the exact binding mechanism of different arsenic species on the surfaces, various spectroscopic studies are required such as Raman spectroscopy, Fourier-transform infrared spectroscopy (FTIR), and X-ray photoelectron spectroscopy (XPS). These studies too have limitations due to the difficulty in understanding adsorbed species in water and the mode of complexation onto the surfaces. To understand the complexation of arsenic onto oxides, some efforts have been made by Gustafsson et al.¹⁷ using computational methods. Authors have used the Diffuse Layer Model (DLM)¹⁸ and Three-Plane CD-MUSIC Model (TPCD)¹⁹ to account for the data. It has been seen that at different pH conditions, both As(III) and As(V) exist as different species.^{20,21} These species bind on different adsorbents

Received: March 17, 2018

Revised: June 4, 2018

Published: June 11, 2018

differently,^{22–25} which also depend on the concentration of the species.^{23,26}

Adsorption of As(III) and As(V) on amorphous aluminum and iron oxides using vibrational spectroscopy was investigated by Goldberg et al.²⁰ According to the report, Al–O–As stretching frequency appeared between 844 to 865 cm^{-1} for pH 5–9, while Fe–O–As frequency was observed between 817 to 824 cm^{-1} for pH 5–10.5. Arsenate forms inner sphere complexes on both amorphous Al and Fe oxides, while As(III) forms inner and outer sphere complexes on amorphous Fe oxide and only outer sphere complexes on amorphous Al oxide. Arsenic speciation in the aqueous phase was studied in detail using Raman spectroscopy by Müller et al.²¹ They studied the binding mechanism of As(III) and As(V) on 2-line ferrihydrite, goethite, hematite, and ferrioxhyte using Raman and diffuse reflectance infrared Fourier-transform (DRIFT) spectroscopy. In solution phase, As(III) and As(V) showed various Raman features. However, the As(III/V) adsorbed samples of ferrihydrite and ferrioxhyte showed Raman feature of Fe–O–As as a broad band, centered around 840 cm^{-1} at pH 5.5 and 9. In the case of As(V), this band was more intense and better resolved than As(III). To know the oxidation state of As, extended X-ray absorption fine structure (EXAFS) spectroscopy was performed which confirmed that no change occurred in the oxidation state of As(III) and As(V) after adsorption. EXAFS and X-ray absorption near edge structure (XANES) spectroscopy studies were widely used to know the mode of complexation of arsenic species on iron oxide/oxyhydroxide.

Wang et al.²² investigated the surface speciation of As(III) and As(V) on green rust by EXAFS and XANES spectroscopies. They found polymeric species of As(III) on the surface of green rust. Bhandari et al.²⁷ studied the effect of light on ferrihydrite with As(III) at pH 5 using XANES and attenuated total reflection-FTIR (ATR-FTIR) spectroscopy. They observed the oxidation of As(III) which was bound to the surface of ferrihydrite. During the adsorption process, the release of Fe(II) ions into solution from ferrihydrite was noticed. Nguema et al.²⁸ performed As(III) sorption with 2-line ferrihydrite, hematite, goethite and lepidocrocite using EXAFS and XANES spectroscopies. They found bidentate binuclear corner sharing (²C) complexes in all cases but bidentate mononuclear edge sharing (²E) complexes additionally for ferrihydrite and hematite. In the environment, the known polymorphs of iron oxides/hydroxides/oxyhydroxides are about sixteen.²⁹ Hematite ($\alpha\text{-Fe}_2\text{O}_3$), magnetite (Fe_3O_4), goethite ($\alpha\text{-FeOOH}$), and ferrihydrite ($\text{Fe}_2\text{O}_3\cdot 0.5\text{H}_2\text{O}$) are the commonly available polymorphs and are used for various industrial and scientific applications. Hematite (HEM), magnetite (MAG), and ferrihydrite (Fh)-based materials were used extensively in water purification for the removal of heavy metal ions (Pb and As).^{30–32} Higher surface area of iron oxides favors larger adsorption capacity for arsenate.³³ Iron oxide nanoparticles are also effective for the removal of other metals such as V, Cr, Co, Mn, Se, Mo, Cd, Sb, Tl, Th, and U.³⁴ Use of nanoadsorbents for the removal of heavy metal ions from water is particularly attractive as they can be altered suitably to achieve greater surface area and stronger binding capacity. Magnetite nanoparticles have certain advantages due to their superparamagnetic properties, ease of preparation, and biocompatibility. However, agglomeration and the loss of magnetic strength over time resulting from auto-oxidation limits the commercial application of bare iron oxide nano-

particles.^{35,36} We had introduced a low cost engineered nanomaterial, named as confined metastable 2-line ferrihydrite (CM2LF), having a high adsorption capacity of 100 mg/g ³⁷ as a solution for arsenic contamination in drinking water. Detailed characterization, comparison with other materials, batch and cartridge studies, mechanical properties, regeneration, reuse, and post adsorption characterization have been reported earlier by Kumar et al.³⁷ The material has been implemented in various parts of West Bengal, Uttar Pradesh, Karnataka, and Punjab states of India for arsenic removal with continuous monitoring, and the technology has reached over 600 000 people now.

Present work mainly focuses on the adsorption kinetics of common As species (H_3AsO_3 , $\text{H}_2\text{AsO}_4^{1-}$, and HAsO_4^{2-}) which exist at pH 7. The oxidation state of iron in CM2LF, MAG, and HEM upon complexation with As species was studied using XPS. The mode of adsorption of various species on these adsorbents was studied using FTIR spectroscopy. Based on these, a mechanistic model of complexation on nanoscale materials was developed.

■ EXPERIMENTAL SECTION

Stock solutions of 100 mM As(III) and As(V) were prepared using NaAsO_2 and $\text{Na}_2\text{HAsO}_4\cdot 7\text{H}_2\text{O}$, respectively. A combination of As(III) and As(V) is referred to as As(mix). A stock solution of 100 mM As(mix) solution was prepared by mixing equimolar amounts of NaAsO_2 and $\text{Na}_2\text{HAsO}_4\cdot 7\text{H}_2\text{O}$. The pH of the stock solutions was adjusted to 7 by adding diluted HCl and diluted NaOH, whenever necessary.

Further, 200 mg of the material (CM2LF/MAG/HEM) was added to 150 mL of arsenic stock solution (As(III)/As(V)/As(mix)) in a 250 mL polypropylene conical flask. The flask was kept in an orbital shaker for 24 h, until an adsorption equilibrium was reached. The solution was centrifuged and the residue (i.e., the arsenic adsorbed material) was washed several times with deionized water to remove unreacted arsenic species from the surface of the material. Subsequently, the cleaned residue was dried at room temperature and a pellet was made using an IR pelletizer. The pellet was kept in a vacuum desiccator for 48 h for complete drying and also to protect it from the surrounding environment, before performing XPS and IR measurements.

To understand the adsorption kinetics of arsenic, Raman measurements were performed. For this, 3–7 g of the material (CM2LF/MAG/HEM) was added to 40–50 mL of 150 mL of arsenic (As(III)/As(V)/As(mix)) solutions in a 250 mL polypropylene conical flask. The solution was kept in an orbital shaker, and 1 mL of the solution was collected at various time intervals at 5, 10, 15, 20, 40, 60, 90, and 120 min, respectively. The solutions were subjected to centrifugation, immediately after collecting them. The material if any, separated as residue, was discarded and Raman measurements were performed using the supernatant.

In this work, each material, viz., CM2LF/MAG/HEM has been investigated thoroughly for interaction with As(III), As(V), and As(mix), respectively.

Materials. Sodium arsenite (NaAsO_2) and disodium hydrogen arsenate ($\text{Na}_2\text{HAsO}_4\cdot 7\text{H}_2\text{O}$) were purchased from SD Fine Chemicals Limited. Hematite ($\alpha\text{-Fe}_2\text{O}_3$) was purchased from Merck Chemicals Pvt. Ltd., India. Magnetite (Fe_3O_4) was purchased from Alfa Aesar (A Johnson Matthey Company, USA). Sodium hydroxide (NaOH) was purchased from Rankem Glasswares and Chemicals Pvt. Ltd., India. Hydrochloric acid (HCl) was purchased from Merck Life Science Pvt. Ltd., India. All chemicals were of analytical grade and were used without further purification. Deionized (DI) water was used throughout the experiments.

Instrumentation. HRTEM images of the sample were obtained with JEM 3010 (JEOL, Japan) operating at 200 kV (to reduce beam induced damage) with an ultrahigh-resolution polepiece. Samples for

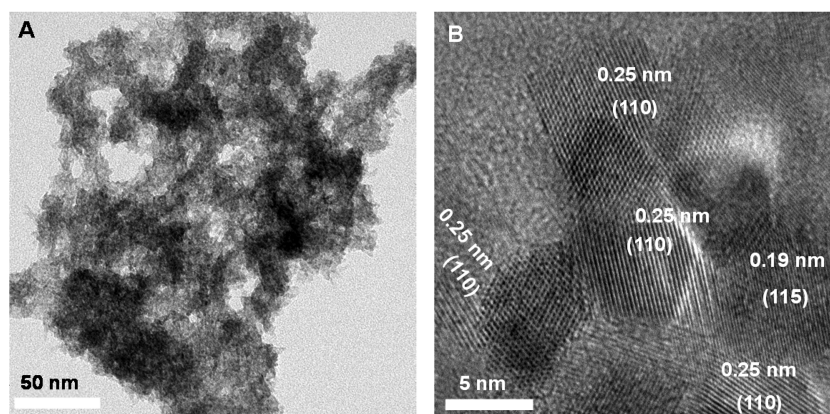


Figure 1. (A) HRTEM image of the 2-line ferrihydrite composite (CM2LF). (B) Lattice resolved image of part A.

HRTEM studies were prepared by dropping the dispersion on amorphous carbon films supported on a copper grid and subsequent drying. XPS measurements were done using an ESCA Probe TPD spectrometer of Omicron Nanotechnology. Polychromatic Al K α was used as the X-ray source ($h\nu = 1486.6$ eV). Samples were mounted as pellets on a carbon tape, supported on the sample stub. Constant analyzer energy of 20 eV was used for the measurements. Binding energy was calibrated with respect to C 1s at 284.8 eV. All the XPS spectra were deconvoluted using CasaXPS software. Raman spectroscopy was performed using CRM Alpha 300 S microRaman spectrometer of WiTec GmbH (Germany). A glass slide with a cavity (which can hold 100 μ L of the sample solution) was mounted on the piezoelectric scan stage of the setup. The spectra were collected at 633 nm laser excitation where a long band-pass filter, placed in the path of signal effectively cuts off the Rayleigh scattering. The signal was then dispersed using a 600 grooves per mm grating, and the dispersed light was collected by a Peltier-cooled charge coupled device. The other parameters of the instrument were kept as integration time, 70 s and accumulation, once. The background subtraction of spectrum was done using a second-order polynomial. All the Raman spectra were deconvoluted using OriginPro 9.0 software. A PerkinElmer FTIR spectrometer was used to measure the infrared spectra. The spectrometer resolution was kept at 4 cm^{-1} . Identification of the phase(s) of CM2LF sample was carried out by XRD (Bruker AXS, D8 Discover, USA) using the Cu K α radiation at $\lambda = 1.5418$ Å. Various model building softwares were used to build the structures. The rectangular slab, nanosphere, and cube were built by using VESTA and Avogadro 1.2.0 software.

RESULTS AND DISCUSSION

Figure 1A shows a TEM image of CM2LF. It appears largely amorphous and continues to remain the same at ambient conditions even after extensive interaction with As(III) and As(V) spiked water. Upon continuous electron beam irradiation, lattice planes are seen under HRTEM due to beam induced crystallization (Figure 1B). Figure S9 shows the XRD data of CM2LF. It shows the 2-line ferrihydrite phase with characteristic features at 35.5° and 62.3° corresponding to the (110) and (115) planes. The observed lattice planes are in agreement with the Cambridge Crystallographic Database (CCD) (JCPDS, 46-1315).^{37–39}

To understand the degree of protonation, polymerization, and speciation of As(III) and As(V) oxides⁴⁰ at room temperature, Raman spectra were measured at pH 7 (Figure 2Aa,Ab). As(III) in solution has two vibrational features at 703 and 656 cm^{-1} (Figure 2Aa) which correspond to the A_1 and E modes of H_3AsO_3 (C_{3v} symmetry when all OH groups are equivalent). The peak at 703 cm^{-1} corresponds to symmetric stretching (A_1) while the other peak at 656 cm^{-1} represents

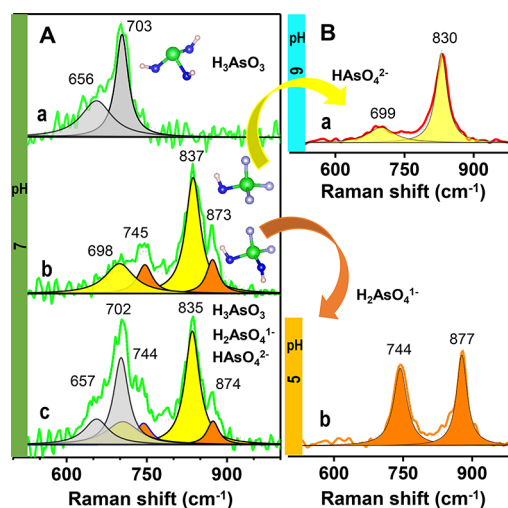


Figure 2. Raman spectra of aqueous arsenite and arsenate species. (A) Data at pH 7 for (a) As(III), (b) As(V), and (c) As(mix). Expanded view of As(V) showing different species at other pH values. (B) Most of the As(V) is in the form of (a) HAsO_4^{2-} at pH 9 and as (b) $\text{H}_2\text{AsO}_4^{1-}$ at pH 5. Data have been fitted with their components.

the asymmetric stretching (E) of As–OH,²¹ respectively. As(V) in solution shows four vibrational features (after deconvolution) at 873, 837, 745, and 698 cm^{-1} (Figure 2Ab). To understand the kind of speciation of As(III) and As(V) in the aqueous phase, we have performed the studies by varying pH, according to the pK_a value of their corresponding acids, and the data are shown in the Supporting Information, Figure S1. As(V) in solution exists as $\text{H}_2\text{AsO}_4^{1-}$ and HAsO_4^{2-} species in the pH window of 5–9, as reported.^{37,20,21} Species $\text{H}_2\text{AsO}_4^{1-}$ and HAsO_4^{2-} belong to C_{2v} (when the OH groups are equivalent) and C_{3v} (when the OH group is considered as a moiety) point groups, respectively. C_{2v} has four vibrational modes, viz., A_1 , A_2 , B_1 , and B_2 while C_{3v} has two vibrational modes, viz., A_1 and E which are Raman active. The vibrational modes of the species $\text{H}_2\text{AsO}_4^{1-}$ and HAsO_4^{2-} were discussed by Müller et al.²¹ As(V) solution was made at pH 5 and pH 9, separately. At pH 9, it shows two features at 830 and 699 cm^{-1} (Figure 2Ba) whereas at pH 5, they were observed at 877 and 744 cm^{-1} (Figure 2Bb). The higher frequency peaks of the spectra (at 830 and 877 cm^{-1}) correspond to the symmetric stretching of As=O, while the lower frequency peaks (699 and 744 cm^{-1}) represent the symmetric stretching of As–OH, respectively. With this explanation, we can assign the Figure

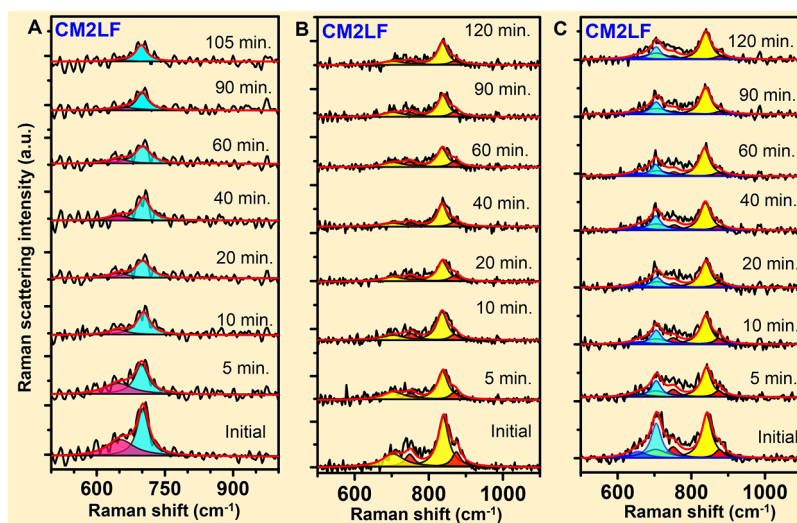


Figure 3. Time dependent Raman spectra of the interaction of CM2LF with (A) As(III), (B) As(V), and (C) As(mix).

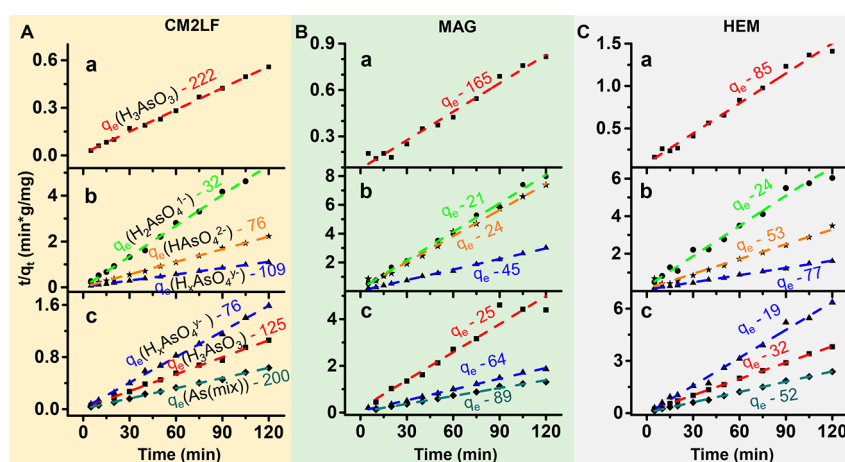


Figure 4. Pseudo-second-order kinetics graph for (A) CM2LF, (B) MAG, and (C) HEM, where plots a, b, and c represent As(III), As(V), and As(mix) removal, respectively. The unit of q_e and q_t is mg/g. The q_t of each data point was evaluated using eq 3 of Supporting Information 4.

2Ab vibrational frequencies 837, 698 and 873, 745 cm^{-1} to HAsO_4^{2-} and $\text{H}_2\text{AsO}_4^{1-}$, respectively. In the case of As(mix) in solution, at pH 7, the observed six vibrational features (after deconvolution) are almost close to the vibrational frequencies of the individual As(III) and As(V) species (H_3AsO_3 , HAsO_4^{2-} , and $\text{H}_2\text{AsO}_4^{1-}$) as discussed earlier. We did not see any additional features which also confirm that there are no adsorption between As(III) and As(V) in solution as a result of mixing. Further details about As–O or As–OH stretching frequencies of arsenic oxides are discussed in Goldberg et al.²⁰

The adsorption kinetics of various arsenic species in solution at pH 7 was studied for different materials, CM2LF, MAG, and HEM. The intensities of As(III), As(V), and As(mix) species decreased upon interaction with CM2LF with time, as shown in Figure 3. Similar decay in intensities of the arsenic species is seen in the case of MAG and HEM as shown in the Supporting Information, Figures S2 and S3, respectively. The data suggest that upon interaction with CM2LF, MAG, and HEM, the arsenic species in solution remained the same. Area under the peaks correspond to concentration in solution, and the data suggest that equilibrium is reached in 20 min as shown in Figure S4. The kinetic graphs in Figure S4A,B follow a pseudo-second-order expression. The similar data for MAG and HEM

are shown in Figures S5 and S6, respectively. We observed that the concentration of As(III) and As(V) in solution reduced faster for CM2LF but not for MAG and HEM. Appropriate analyses of the data are presented in the Supporting Information.

Raman measurements of various concentrations of As(III) and As(V) are shown in the Supporting Information, Figure S7A,B, respectively. The correlation between the area under the peak and the concentration of As(III) and As(V) solutions are shown in Figure S7C,D, respectively. To understand the adsorption kinetics and uptake capacity, we plotted t/q_t versus t (Figure 4); the rate constants (k) and adsorption capacity (q_e) of all the materials were calculated using the slopes and intercepts of the plots. The results are tabulated in Table 1. Similar adsorption models for the uptake of arsenic have been reported earlier.^{9,30,41}

The obtained rate constants for CM2LF and HEM are equal for As(III) adsorption but less for MAG (Table 1). We assume that this may be due to the difference in availability of surface $-\text{O}^-/-\text{OH}$ groups on all three materials. While in the case of As(V), MAG shows faster kinetics in comparison to CM2LF and HEM, even though it shows less uptake of As(V). As we know that As(V) in solution exists as $\text{H}_2\text{AsO}_4^{1-}$ and HAsO_4^{2-}

Table 1. Adsorption Data in Terms of Initial Rates, Rate Constants, and Uptake of As at Equilibrium

adsorbate 150 mL	adsorbent (g)	species pH 7	q_e (mg/g) \pm 5%	k (min(mg/g)) ⁻¹ \pm 5%	initial rate $h = kq_e^2 \pm 10\%$	R^2
50 mM As(III)	CM2LF : 3 g	H ₃ AsO ₃	222	1.5×10^{-3}	74	0.99
	MAG : 3 g	H ₃ AsO ₃	165	0.4×10^{-3}	11	0.99
	HEM : 3 g	H ₃ AsO ₃	85	1.5×10^{-3}	11	0.99
40 mM As(V)	CM2LF : 7 g	H _x AsO ₄ ^{y-}	109	5.0×10^{-3}	59	0.99
		H ₂ AsO ₄ ¹⁻	32	60.0×10^{-3}	61	0.99
		HAsO ₄ ²⁻	76	20.0×10^{-3}	115	0.99
	MAG : 7 g	H _x AsO ₄ ^{y-}	45	19.0×10^{-3}	38	0.98
		H ₂ AsO ₄ ¹⁻	21	25.0×10^{-3}	11	0.98
		HAsO ₄ ²⁻	24	17.0×10^{-3}	10	0.98
	HEM : 7 g	H _x AsO ₄ ^{y-}	77	2.0×10^{-3}	12	0.98
		H ₂ AsO ₄ ¹⁻	24	12.0×10^{-3}	7	0.98
		HAsO ₄ ²⁻	53	4.5×10^{-3}	13	0.98
50 mM As(mix)	CM2LF : 5 g	As(mix)	200	3.0×10^{-3}	120	0.99
		H ₃ AsO ₃	125	7.0×10^{-3}	109	0.99
		H _x AsO ₄ ^{y-}	76	8.5×10^{-3}	49	0.99
	MAG : 5 g	As(mix)	89	4.0×10^{-3}	32	0.99
		H ₃ AsO ₃	25	5.0×10^{-3}	31	0.95
		H _x AsO ₄ ^{y-}	64	12.0×10^{-3}	49	0.99
	HEM : 5 g	As(mix)	52	13.0×10^{-3}	35	0.99
		H ₃ AsO ₃	32	13.0×10^{-3}	13	0.99
		H _x AsO ₄ ^{y-}	20	40.0×10^{-3}	16	0.97

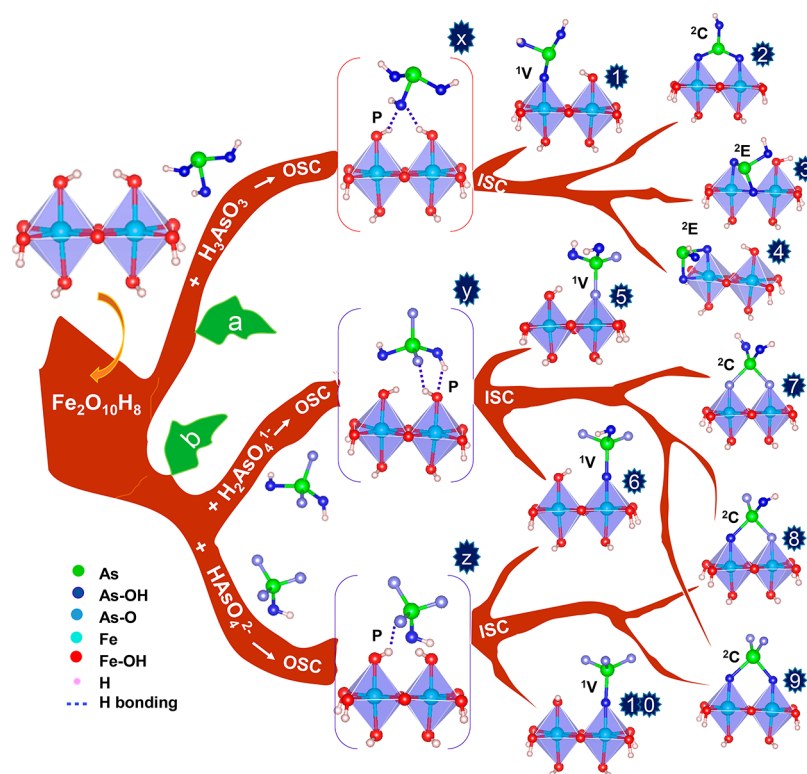


Figure 5. A model of As complexes with Fe₂O₁₀H₈ cluster. Path a, As(III) complexes and path b, As(V) complexes. OSC, outer sphere complexes (x, y, and z). ISC, inner sphere complexes (1 to 10). Transformation of OSC to ISC by ligand exchange is shown.

at pH 7, we were interested to know which species will have faster kinetics toward iron oxides/oxyhydroxides. Data of Table 1 reveal that H₂AsO₄¹⁻ shows higher rate constant than HAsO₄²⁻ for CM2LF, MAG, and HEM at pH 7 irrespective of their different surface structures. Further studies were conducted using As(mix) and As(V), which showed higher

rate constant than As(III). Thus, As(V) interaction with all the materials is faster in comparison to As(III) due to the difference in the species in the solution phase. As(V) shows faster adsorption kinetics as compared to As(III). It is due to As(V) (H₂AsO₄¹⁻/HAsO₄²⁻) possessing more polarizable hydration sphere than As(III) (H₃AsO₃). Nucleophilicity

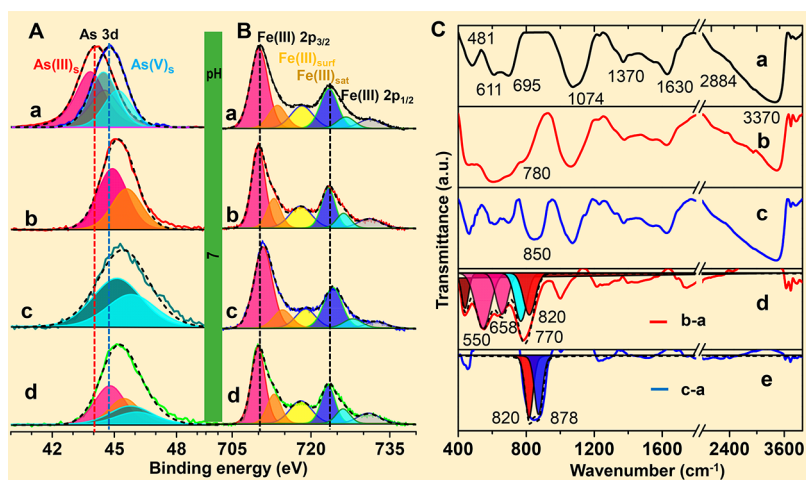


Figure 6. XPS spectrum of (A) As 3d and (B) Fe 2p. As 3d region of (A) (a) NaAsO_2 (red trace) and $\text{Na}_2\text{HASO}_4 \cdot 7\text{H}_2\text{O}$ (blue trace). Comparison of the positions may be noted. (b) As(III), (c) As(V), and (d) As(mix) adsorbed on CM2LF. Spectra are fitted for the $3d_{5/2}$ and $3d_{3/2}$ features. (B) (a) CM2LF before adsorption, (b–d) Fe 2p after adsorption, as before. (C) FTIR spectra (a) CM2LF before adsorption. Spectra of (b) As(III) and (c) As(V) adsorbed materials. (d) Spectra after subtraction (curve b-a). (e) Spectra after subtraction (curve c-a).

plays an important role in the inner sphere complexation process (ligand exchange mechanism). More nucleophilic ligands ($-\text{O}^- > -\text{OH}$) can easily replace the labile groups ($-\text{OH}/\text{H}_2\text{O}^+-$). In acidic pH, most of the singly coordinated oxygens are present on the surface of adsorbent in the form of $\text{H}_2\text{O}^+/-\text{OH}$ groups. As the pH becomes basic, the singly coordinated oxygens change to $-\text{OH}/-\text{O}^-$. Thus, at pH 7, the surface of adsorbent can be composed of $\text{H}_2\text{O}^+/-\text{O}^-/-\text{OH}$ groups. Repulsions existing between $\text{Fe}-\text{O}^-$ (adsorbent) and $\text{As}-\text{O}^-$ (adsorbate) groups are the cause of reduced adsorption of As(V) than As(III). As(V) has more nucleophilic ligands ($-\text{As}-\text{O}^-$) as compared to As(III) ($-\text{As}-\text{OH}$). Thus, we can conclude that nucleophilicity is one of the key factors leading to faster adsorption kinetics for As(V) than As(III) at pH 7. The effect of nucleophilicity of ligands and the difference in molecular basis of the adsorption process for As(III) and As(V) are shown in Figure S10.

Adsorption at equilibrium has shown that As(III) uptake is higher than As(V) for CM2LF and HEM (Table 1) and not for MAG. We believe that decrease in availability of adsorption sites for As(III) due to the initial occupation of them by As(V) and also pH of the solution are the major reasons for reduced uptake by MAG. Among the adsorbents studied, the rate constant is highest for MAG for As(V) uptake. It also shows the lowest rate constant for As(III) uptake (Table 1).

Effect of Competing Ions. We further studied the influence of competing ions on arsenic adsorption for CM2LF, MAG, and HEM to improve the application of materials for point-of-use water purification. We have considered the ions which are generally present in natural water: NO_3^- , CO_3^{2-} , PO_4^{3-} , SO_4^{2-} , Cl^- , and HCO_3^- and performed experiments for As(III) and As(V), separately. As(III) adsorption was more than that of As(V) for all the materials. The corresponding data are shown in Figure S11. CM2LF removes As(III) and As(V) effectively as compared to MAG and HEM even in the presence of competing ions. The data show that the influence of PO_4^{3-} ion was considerably higher than that of other ions for all the materials.

In the following, we present a model for the adsorption of arsenic species on CM2LF based on the data available. For this model, a unit of the substrate is considered. For FeOOH based

materials, the $\text{Fe}_2\text{O}_{10}\text{H}_8$ unit, an edge share hydroxyl terminated bioctahedron is taken as the model system. Possible complexes that can be formed via ligand exchange mechanism upon the adsorption of As(III) and As(V) on this model cluster at pH 7 are shown in Figure 5. We may recall that the Fe_2O_{10} cluster is the common unit (two octahedra present in edge sharing fashion) of 2-line ferrihydrite, MAG and HEM. The oxide upon exposure to water will have hydroxylated surfaces making this model realistic. There are two kinds of adsorption geometries (physical and chemical) possible in the case of As species. Physical adsorption leads to outer sphere (physically bonded species (P) through hydrogen bonding) complexes while chemical adsorption result in inner sphere (chemically bonded) complexes. Most of the outer sphere complexes can transform to inner sphere complexes through ligand exchange mechanism as indicated by the pathways (“path a” and “path b”). In Figure 5, x, y and z represent the outer sphere complexes formed through hydrogen bonding between As species and iron oxides/oxyhydroxides as reported.^{26,42} The inner sphere complexes are (1) monodentate mononuclear (¹V), (2) bidentate binuclear corner sharing (²C), and (3) bidentate mononuclear/binuclear edge sharing (²E). The ratio of outer to inner sphere complexes depend on the pH of the solution.^{23,26} Complex 2 from Figure 5 (“path a”) and complexes 7, 8, and 9 from Figure 5 (“path b”) represent the ²C complexes. The complexes 7, 8, and 9 are structurally similar and differ in the degree of protonation of As(V) species. As(III) and As(V) have more tendency to form ²C complexes (thermodynamically favorable) than other possible structures^{28,43,44} for all the adsorbents used in this work. Bidentate mononuclear edge sharing (²E) complexes were found in the case of As(III) with ferrihydrite and HEM.²⁸ Complex 1 from Figure 5 (“path a”) and complexes 5, 6, and 10 from Figure 5 (“path b”) show monodentate mononuclear (¹V) complexes. These are found to increase in intensity noticeably at pH 7–10^{23,22} in the case of As(III) and at pH 5–10^{26,42} in the case of As(V) with iron oxides/oxyhydroxides.

The XPS analysis of arsenic standards in the solid form (As(III)_s and As(V)_s, subscript “s” refers to solid state) are shown in Figure 6Aa, 7Aa, and Figure S8Aa. The measurements were done using standard arsenic compounds viz.,

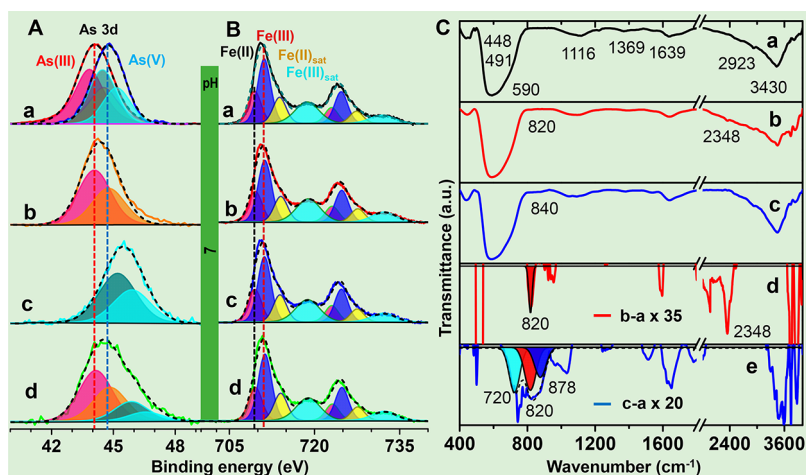


Figure 7. XPS spectrum of (A) As 3d and (B) Fe 2p. As 3d region of (A) (a) NaAsO_2 (red trace) and $\text{Na}_2\text{HAsO}_4 \cdot 7\text{H}_2\text{O}$ (blue trace). Comparison of the positions may be noted. (b) As(III), (c) As(V), and (d) As(mix) adsorbed on MAG. Spectra are fitted for the $3d_{5/2}$ and $3d_{3/2}$ features. (B) (a) MAG before adsorption, (b, c, and d) Fe 2p after adsorption, as before. (C) FTIR spectra (a) MAG before adsorption. Spectra of (b) As(III) and (c) As(V) adsorbed materials. (d) Spectra after subtraction (curve b-a). (e) Spectra after subtraction (curve c-a).

NaAsO_2 for As(III) and Na_2HAsO_4 for As(V). The As 3d peak appears at 44.2 and 44.8 eV for As(III)_s and As(V)_s , respectively.⁴⁵ The As 3d peak was deconvoluted into $3d_{5/2}$ and $3d_{3/2}$, while Fe 2p was fitted with three pairs of peaks for CM2LF and HEM as reported.^{46,47} The lower binding energy peak corresponds to $-\text{Fe}-\text{O}-\text{Fe}-$ groups, the next higher one refers to surface $>\text{Fe}-\text{OH}$ groups ($\text{Fe(III)}_{\text{surf}}$) followed by a satellite peak ($\text{Fe(III)}_{\text{sat}}$).⁴⁶ XPS data of each peak before and after arsenic (As(III) , As(V) , and As(mix)) interaction with all three materials used in this work are shown in Table S1. The standard As 3d peak was redshifted from 44.2 to 45.1 and 44.7 eV upon As(III) interaction with CM2LF (Figure 6Ab) and HEM (Supporting Information, Figure S8Ab), respectively. The observed results suggest that most of the H_3AsO_3 species on the surface of CM2LF and HEM are chemically bonded or may have got converted to As(V). In the case of As(V) adsorption on CM2LF and HEM, the As 3d peak redshifts from a value of 44.8 to 45.3 and 46.5 eV for CM2LF (Figure 6Ac) and HEM (Supporting Information, Figure S8Ac), respectively. The redshift of As 3d peak was higher in the case of HEM and lower for CM2LF (broaden to higher binding energy side). Lower redshift can refer to physically adsorbed and higher redshift can suggest chemically adsorbed species. The FTIR characteristic features of CM2LF before arsenic adsorption (Figure 6Ca) shows Fe–O stretching frequencies of 2-line ferrihydrite at 481, 611, and 695 cm^{-1} , respectively. Peaks at 1074, 1370, and 3370 cm^{-1} are due to asymmetric C–O–C stretching, N–H deformation, and N–H stretching of chitosan (the polymer used to make CM2LF), respectively. The C=O stretching of amide and C–H stretching of the polymer were noticed at 1630 and 2884 cm^{-1} , respectively, as reported by Kumar et al.³⁷ The peak at 3370 cm^{-1} suggest the stretching vibrations of adsorbed water and hydroxyl groups of CM2LF. The free H_3AsO_3 molecules in water show stretching vibrations of As–OH at 703 and 656 cm^{-1} (Figure 2Aa), which gives a new peak at 780 cm^{-1} upon interaction with CM2LF^{26,28} due to which enhancement of Fe–O peaks of CM2LF was observed in the 600–700 cm^{-1} region. The enhancement may be due to the overlap of H_3AsO_3 (As–OH) stretching vibrations and Fe–O vibrations of CM2LF. This effect can be noticed from the subtracted

spectrum, curve b-a of Figure 6Cd. The fitted curve b-a shows the adsorbed H_3AsO_3 features at 550, 658, and 770 cm^{-1} . The 770 cm^{-1} is due to chemically adsorbed species and the other two, 550 and 658 cm^{-1} suggest physically adsorbed (hydrogen bonded) H_3AsO_3 (As–OH stretching) on CM2LF. The results were supported by the work of Sverjensky et al.²³ and Fukushi et al.²⁶ These authors studied arsenic speciation on ferrihydrite surface using IR and extended X-ray adsorption fine structure (EXAFS) spectroscopies and applied the extended triple layer model (ETLM). The ^{23}C complexes dominate than the ^{13}C and ^{31}P complexes for As(III) and As(V). In the present study, the ratio of physical to chemical adsorption is more for As(V) than for As(III) due to difference in the extent of deprotonation of arsenic species and increase of $-\text{O}^-$ groups on the surface of the adsorbent. The results suggest that the effect of pH is more on As(V) than As(III).

In the case of MAG, the Fe $2p_{3/2}$ was deconvoluted into four peaks which correspond to Fe(II), Fe(III) and two separate shakeup peaks for Fe(II) ($\text{Fe(II)}_{\text{sat}}$) and Fe(III) ($\text{Fe(III)}_{\text{sat}}$), respectively.^{46,48} Similarly, the deconvolution was done for Fe $2p_{1/2}$. Upon As(III) interaction with MAG, no considerable change was observed in As 3d. The peak shifted from 44.2 to 44.3 eV (Figure 7Ab) while in the case of As(V), it redshifted from 44.8 to 45.5 eV (Figure 7Ac). Thus, we can conclude that most of the H_3AsO_3 species are physically adsorbed and $\text{H}_x\text{AsO}_4^{y-}$ species are chemically adsorbed on MAG. In both the cases, there was no considerable change in peak positions, intensity ratio, and fwhm of Fe(II) and Fe(III). These suggest that there was no conversion of Fe(II) to Fe(III) and vice versa. The characteristic features of MAG in FTIR before arsenic exposure (Figure 7Ca) shows the Fe–O stretching frequencies at 448, 491, and 590 cm^{-1} , respectively. Peaks at 1639 and 3430 cm^{-1} are due to bending and stretching vibrations of adsorbed water on MAG. Peak at 2348 cm^{-1} is due to free CO_2 in the spectrometer.

A peak at 820 cm^{-1} was found upon interaction of As(III) and As(V) with CM2LF and MAG. This feature due to Fe–O–As stretching vibrations of the bidentate binuclear (^{23}C) complex⁴⁹ occurs in the range of pH 7 to 9, which confirms that the arsenic species (H_3AsO_3 and $\text{H}_2\text{AsO}_4^{1-}$ and HAsO_4^{2-}) are forming the inner sphere complexes on the surface of these

Table 2. Correlation of Adsorption Models and Spectroscopic Data

adsorbate pH 7	adsorbent	As 3d shift (eV)	Fe 2p _{3/2} shift (eV)	IR features (cm ⁻¹)	suggested complexes ^a
As(III) (H ₃ AsO ₃)	CM2LF	+ 0.9	0.1	820	complex 2
				550, 658	complex x
	MAG	+ 0.1	0		complex x
	HEM	+ 0.5	- 0.2	820	complex 2/1 may be complex 2
As(V) (HAsO ₄ ²⁻ / H ₂ AsO ₄ ¹⁻)	CM2LF	+ 0.5	+ 0.1	820	complex (7/8/9)
	MAG	+ 0.7	+ 0.3	820	complex (7/8/9)
	HEM	+ 1.5	- 0.2	720	complex (y and z) complex (7/8/9)

^aComplexes refer to those in Figure 5, assigned on the basis of FTIR features and As 3d peak shift values.

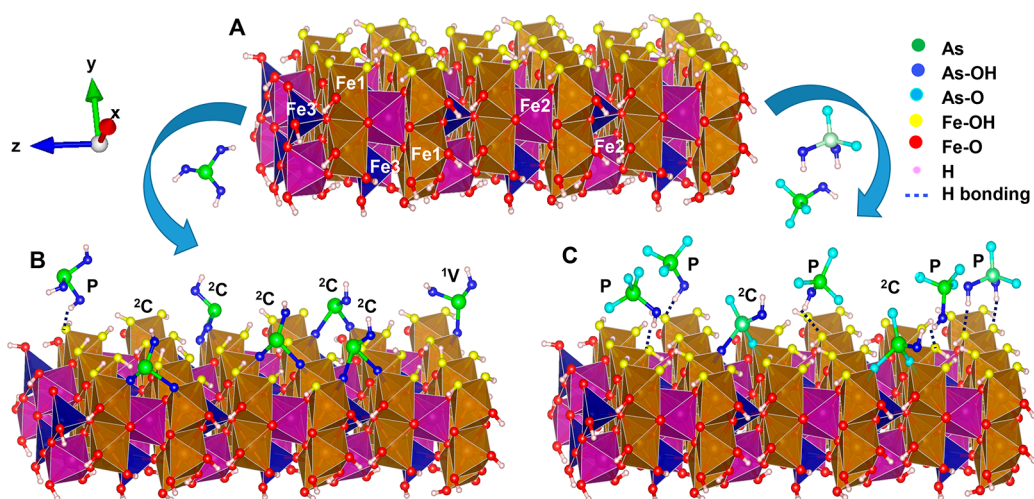


Figure 8. Schematic of a 110 plane of ferrihydrite at pH 7 (A) before adsorption, (B) after As(III) adsorption, and (C) after As(V) adsorption.

materials. CM2LF and MAG show a special feature at 878 cm⁻¹ after As(V) adsorption which represents the As=O stretching vibrations⁴⁹ of H_xAsO₄^{y-}. Figures 6Ad, 7Ad, and Figure S8Ad show that As(III) is more interactive than As(V) at pH 7, in the case of As(mix). The results were supported by Raman data (Table 1). The correlation of adsorption models (Figure 5) and spectroscopic data (XPS and IR) based on the present work is summarized in Table 2.

The XPS data (Table 2) suggest that there is no considerable change in Fe 2p upon interaction with arsenic (As(III)/As(V)), which implies that the Fe atoms involved in the complexation did not undergo any chemical change for all the materials reported in this work. We assume that formation of the complexes follows the ligand exchange mechanism. The stability of the complexation of arsenic species with ferric hydroxides was reported by Farrell et al.⁴² The stability of the complexes is in the order: bidentate binuclear (>(FeO)₂AsOH ≈ ²C) > monodentate mononuclear (>(FeO)-As(OH)₂ ≈ ¹V) > physical adsorption (P).

In the following, we discuss an understanding of the adsorption of arsenic species on CM2LF. In Figure 8, we used the unit cell parameters of 2-line ferrihydrite as reported in Michel et al.^{39,50} to construct a rectangular slab having top and bottom surfaces parallel to the (110) plane of FeOOH (Figure 8A). The top surface contains oxygen atoms (in yellow). In general, the ferrihydrite structure has three symmetry-distinct Fe atoms. Here, we represented them as octahedra Fe1 center (dark yellow), octahedra Fe2 center (indigo), and tetrahedra

Fe3 center (blue) as reported by Pinney et al.⁵⁰ The CM2LF -O⁻/₋OH groups were shown in yellow/red, while arsenic attached -O⁻ and -OH groups are marked in sky blue and blue, respectively. XPS and FTIR results suggest that arsenic species bind the surface Fe atoms through a ligand exchange mechanism, at pH 7. The results are supported by the literature.^{23,21,24,25,20,26} In the ligand exchange mechanism, As-O⁻/₋OH groups replace the Fe-O⁻/₋OH groups. The formation of possible stable complexes of As(III) and As(V) with 2-line ferrihydrite are shown in Figure 8B,C, respectively. As(III) forms ²C (major) and ¹V (minor) complexes while As(V) forms ²C, ¹V (minor) and P (major) complexes.

We generated a 2-line ferrihydrite nanosphere of 2.6 nm in diameter (Figure 9A) and constructed a cube (Figure 9B) such that the surface area of the cube equals the surface area of the nanosphere ($6a^2 = 4\pi r^2$). The diameter chosen was to simulate the experiment. Possible sites for adsorption were counted as the number of singly coordinated oxy/hydroxy (Fe-O⁻/₋OH) groups from Fe1 (octahedral, blue color) and Fe2 (octahedral, yellow color) centers available on the surface of the nanosphere and cube. Only one site was counted if more than one site was present on the same center due to possible steric hindrance of the complexed species. Ideally, 86 sites were counted for the nanosphere and 54 sites were possible for the cube. We applied two constraints to get maximum arsenic uptake capacity of 2-line ferrihydrite. (1) All the particles (nanosphere or cube) were assumed to be well separated to make all the sites available for adsorption and (2) all the

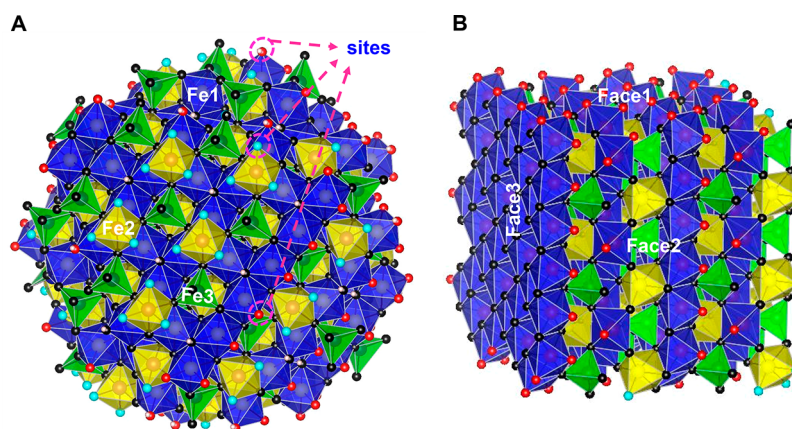


Figure 9. A generated nanosphere model of 2.6 nm diameter by using the unit cell parameters of 2-line ferrihydrite. Singly coordinated oxygens attached to the Fe1 and Fe2 centers are represented with red and sky blue colors, respectively. (B) A cube of the same sample using the information presented. We developed a model of a cubic particle of FeOOH with arsenic adsorption, such that its surface area is equal to the surface area of a 2.6 nm sphere.

arsenic species were attached to the surface Fe atoms as monodentate mononuclear (¹V) or bidentate mononuclear in an edge sharing (²E) fashion assuming that one arsenic species should occupy one site and the other possible complexes (bidentate binuclear (²C) and physical adsorption (P)) were excluded. The density of 2.6 nm particle is 3.5 g/cm³ as reported.⁵¹ Correspondingly, 32.21×10^{-21} g and 23.25×10^{-21} g are the masses of a single nanosphere and a cube, respectively, which are calculated using density and volume of the specific geometry (here the density of nanosphere and cube were assumed as equal). Further, 3.1×10^{19} nanospheres or 4.3×10^{19} cubes are needed to make 1 g of 2-line ferrihydrite. The total number of sites available on nanospheres ($3.1 \times 10^{19} \times 86 = 2.666 \times 10^{21} = 4.426 \times 10^{-3}$ moles of sites) or cubes ($4.3 \times 10^{19} \times 54 = 2.322 \times 10^{21} = 3.856 \times 10^{-3}$ moles of sites) for 1 g of 2-line ferrihydrite were calculated. In the case of nanospheres, ideally, the maximum adsorption capacities for As(III) and As(V) were about 557 and 620 mg/g (where all the sites fully occupied by H₃AsO₃ or H_xAsO₄^{y-} species), respectively, while in the case of cubes, they were about 485 and 543 mg/g for As(III) and As(V), respectively. The theoretical calculations suggest that the shape and geometry of nanoparticle present in 2-line ferrihydrite can profoundly affect its uptake capacity. The experimental uptake capacity could reach almost half of the theoretical value.

CONCLUSIONS

Species-dependent arsenic adsorption on iron oxides/oxyhydroxides was investigated by Raman spectroscopy. Time dependent Raman measurements allowed us to understand an effective material for better arsenic uptake for various species, H₂AsO₄¹⁻ and HAsO₄²⁻, at neutral pH. The studies suggested that their complexation with iron oxides/oxyhydroxides was driven by the ligand exchange mechanism which could lead to the formation of Fe–O–As bonds at neutral pH. Complementary data were obtained from vibrational spectroscopy. CM2LF showed the highest arsenic adsorption capacity than the commonly available polymorphs of iron oxides (MAG and HEM) at neutral pH. CM2LF showed effective removal of As(III) and As(V) in natural waters which supported its use in point-of-use water purification applications. Using the adsorption kinetics, understanding of the species present on the surfaces and speciation of arsenite and arsenate ions known

previously, a model of an arsenic adsorbed nanoparticle of FeOOH was arrived at. This model explains observed results accurately.

ASSOCIATED CONTENT

Supporting Information

The Supporting Information is available free of charge on the ACS Publications website at DOI: [10.1021/acssuschemeng.8b01217](https://doi.org/10.1021/acssuschemeng.8b01217).

Aqueous Raman spectra of arsenic speciation under various pH conditions; time dependent Raman spectra for the interaction of MAG and HEM with As species; representation of data in terms of area under the peak and concentration of species with time; XPS spectra of As 3d and Fe 2p before and after arsenic adsorption; XRD pattern of CM2LF; molecular basis model of the adsorption process; effect of competing ions on arsenic adsorption (PDF)

AUTHOR INFORMATION

Corresponding Author

*E-mail: pradeep@iitm.ac.in. Phone: +91-44 2257 4208. Fax: +91-44 2257 0545/0509.

ORCID

Avula Anil Kumar: [0000-0001-6878-8736](https://orcid.org/0000-0001-6878-8736)

Thalappil Pradeep: [0000-0003-3174-534X](https://orcid.org/0000-0003-3174-534X)

Notes

The authors declare no competing financial interest.

ACKNOWLEDGMENTS

The authors thank Mohd. Azhardin Ganayee and Tripti Ahuja for their technical support in conducting the Raman measurements. The authors also thank Ganesan Paramasivam for his help in constructing a 2.6 nm sphere of 2-line ferrihydrite. Radha Gobinda Bhui who is currently working at University Erlangen-Nürnberg, Egerlandstrasse, Germany, Sophisticated Analytical Instrument Facility at IIT Madras is thanked for the FTIR measurements. The authors thank the Department of Science and Technology (Government of India) for constantly supporting our research program on nanomaterials.

REFERENCES

- (1) *Guidelines for Drinking-Water Quality*; WHO Press, World Health Organization: Switzerland, 2011.
- (2) Amini, M.; Abbaspour, K. C.; Berg, M.; Winkel, L.; Hug, S. J.; Hoehn, E.; Yang, H.; Johnson, C. A. Statistical modeling of global geogenic arsenic contamination in groundwater. *Environ. Sci. Technol.* **2008**, *42* (10), 3669.
- (3) Bhattacharya, P.; Polya, D.; Jovanovic, D., Eds. *Best Practice Guide on the Control of Arsenic in Drinking Water*; IWA Publishing: London, 2017; DOI: 10.2166/9781780404929.
- (4) Mahler, J.; Persson, I.; Herbert, R. B. Hydration of arsenic oxyacid species. *Dalton Transactions* **2013**, *42* (5), 1364.
- (5) Yan, W.; Vasic, R.; Frenkel, A. I.; Koel, B. E. Intraparticle reduction of arsenite (As(III)) by nanoscale zerovalent iron (nZVI) investigated with in situ X-ray absorption spectroscopy. *Environ. Sci. Technol.* **2012**, *46* (13), 7018.
- (6) Raven, K. P.; Jain, A.; Loeppert, R. H. Arsenite and arsenate adsorption on ferrihydrite: Kinetics, equilibrium, and adsorption envelopes. *Environ. Sci. Technol.* **1998**, *32* (3), 344.
- (7) Mota, A. M.; Pinheiro, J. P.; Simões Gonçalves, M. L. Electrochemical methods for speciation of trace elements in marine waters. *Dynamic Aspects. J. Phys. Chem. A* **2012**, *116* (25), 6433.
- (8) Ahmad, A.; et al. Arsenic Remediation of Drinking Water: An Overview. In *Best Practice Guide on the Control of Arsenic in Drinking Water*; Bhattacharya, P., Polya, D., Jovanovic, D., Eds.; IWA Publishing: London, 2017; DOI: 10.2166/9781780404929_079.
- (9) Kumar, S.; Nair, R. R.; Pillai, P. B.; Gupta, S. N.; Iyengar, M. A. R.; Sood, A. K. Graphene oxide–MnFe₂O₄ magnetic nanohybrids for efficient removal of lead and arsenic from water. *ACS Appl. Mater. Interfaces* **2014**, *6* (20), 17426.
- (10) Habuda-Stanić, M.; Nujić, M. Arsenic removal by nanoparticles: a review. *Environ. Sci. Pollut. Res.* **2015**, *22* (11), 8094.
- (11) Pena, M.; Meng, X.; Korfiatis, G. P.; Jing, C. Adsorption mechanism of arsenic on nanocrystalline titanium dioxide. *Environ. Sci. Technol.* **2006**, *40* (4), 1257.
- (12) Litter, M. I. Last advances on TiO₂-photocatalytic removal of chromium, uranium and arsenic. *Current Opinion in Green and Sustainable Chemistry* **2017**, *6*, 150.
- (13) Tang, W.; Su, Y.; Li, Q.; Gao, S.; Shang, J. K. Superparamagnetic magnesium ferrite nanoadsorbent for effective arsenic (III, V) removal and easy magnetic separation. *Water Res.* **2013**, *47* (11), 3624.
- (14) Luo, X.; Wang, C.; Wang, L.; Deng, F.; Luo, S.; Tu, X.; Au, C. Nanocomposites of graphene oxide-hydrated zirconium oxide for simultaneous removal of As(III) and As(V) from water. *Chem. Eng. J.* **2013**, *220* (Supplement C), 98.
- (15) La, D. D.; Patwari, J. M.; Jones, L. A.; Antolasic, F.; Bhosale, S. V. Fabrication of a GNP/Fe–Mg binary oxide composite for effective removal of arsenic from aqueous solution. *ACS Omega* **2017**, *2* (1), 218.
- (16) Lin, S.; Yang, H.; Na, Z.; Lin, K. A novel biodegradable arsenic adsorbent by immobilization of iron oxyhydroxide (FeOOH) on the root powder of long-root Eichhornia crassipes. *Chemosphere* **2018**, *192*, 258.
- (17) Gustafsson, J. P.; Bhattacharya, P. Geochemical modelling of arsenic adsorption to oxide surfaces. *Trace Metals and other Contaminants in the Environment* **2007**, *9*, 159.
- (18) Dzombak, D. A.; Morel, F. M. M. *Surface Complexation Modeling: Hydrous Ferric Oxide*; John Wiley and Sons: New York, 1990.
- (19) Hiemstra, T.; Van Riemsdijk, W. H. A surface structural approach to ion adsorption: The charge distribution (CD) model. *J. Colloid Interface Sci.* **1996**, *179* (2), 488.
- (20) Goldberg, S.; Johnston, C. T. Mechanisms of arsenic adsorption on amorphous oxides evaluated using macroscopic measurements, vibrational spectroscopy, and surface complexation modeling. *J. Colloid Interface Sci.* **2001**, *234* (1), 204.
- (21) Müller, K.; Ciminelli, V. S. T.; Dantas, M. S. S.; Willscher, S. A comparative study of As(III) and As(V) in aqueous solutions and adsorbed on iron oxy-hydroxides by Raman spectroscopy. *Water Res.* **2010**, *44* (19), 5660.
- (22) Wang, Y.; Morin, G.; Ona-Nguema, G.; Juillot, F.; Guyot, F.; Calas, G.; Brown, G. E. Evidence for different surface speciation of arsenite and arsenate on green rust: An EXAFS and XANES study. *Environ. Sci. Technol.* **2010**, *44* (1), 109.
- (23) Sverjensky, D. A.; Fukushi, K. A predictive model (ETLM) for As(III) adsorption and surface speciation on oxides consistent with spectroscopic data. *Geochim. Cosmochim. Acta* **2006**, *70* (15), 3778.
- (24) Arts, D.; Abdus Sabur, M.; Al-Abadleh, H. A. Surface interactions of aromatic organoarsenical compounds with hematite nanoparticles using ATR-FTIR: Kinetic studies. *J. Phys. Chem. A* **2013**, *117* (10), 2195.
- (25) ThomasArrigo, L. K.; Mikutta, C.; Byrne, J.; Barmettler, K.; Kappler, A.; Kretzschmar, R. Iron and arsenic speciation and distribution in organic flocs from streambeds of an arsenic-enriched peatland. *Environ. Sci. Technol.* **2014**, *48* (22), 13218.
- (26) Fukushi, K.; Sverjensky, D. A. A predictive model (ETLM) for arsenate adsorption and surface speciation on oxides consistent with spectroscopic and theoretical molecular evidence. *Geochim. Cosmochim. Acta* **2007**, *71* (15), 3717.
- (27) Bhandari, N.; Reeder, R. J.; Strongin, D. R. Photoinduced oxidation of arsenite to arsenate on ferrihydrite. *Environ. Sci. Technol.* **2011**, *45* (7), 2783.
- (28) Ona-Nguema, G.; Morin, G.; Juillot, F.; Calas, G.; Brown, G. E. EXAFS analysis of arsenite adsorption onto two-line ferrihydrite, hematite, goethite, and lepidocrocite. *Environ. Sci. Technol.* **2005**, *39* (23), 9147.
- (29) Jubb, A. M.; Allen, H. C. Vibrational spectroscopic characterization of hematite, maghemite, and magnetite thin films produced by vapor deposition. *ACS Appl. Mater. Interfaces* **2010**, *2* (10), 2804.
- (30) Chandra, V.; Park, J.; Chun, Y.; Lee, J. W.; Hwang, I.-C.; Kim, K. S. Water-dispersible magnetite-reduced graphene oxide composites for arsenic removal. *ACS Nano* **2010**, *4* (7), 3979.
- (31) Rout, K.; Mohapatra, M.; Anand, S. 2-Line ferrihydrite: synthesis, characterization and its adsorption behaviour for removal of Pb(II), Cd(II), Cu(II) and Zn(II) from aqueous solutions. *Dalton Trans.* **2012**, *41* (11), 3302.
- (32) Sengupta, A.; Mallick, S.; Bahadur, D. Tetragonal nanostructured zirconia modified hematite mesoporous composite for efficient adsorption of toxic cations from wastewater. *J. Environ. Chem. Eng.* **2017**, *5* (5), 5285.
- (33) Carabante, I.; Mouzon, J.; Kumpiene, J.; Gran, M.; Fredriksson, A.; Hedlund, J. Reutilization of porous sintered hematite bodies as effective adsorbents for arsenic(V) removal from water. *Ind. Eng. Chem. Res.* **2014**, *53* (32), 12689.
- (34) Shipley, H. J.; Engates, K. E.; Guettner, A. M. Study of iron oxide nanoparticles in soil for remediation of arsenic. *J. Nanopart. Res.* **2011**, *13* (6), 2387.
- (35) Alijani, H.; Shariatnia, Z. Effective aqueous arsenic removal using zero valent iron doped MWCNT synthesized by in situ CVD method using natural α -Fe₂O₃ as a precursor. *Chemosphere* **2017**, *171* (Supplement C), 502.
- (36) Rashid, M.; Sterbinsky, G. E.; Pinilla, M. Á. G.; Cai, Y.; O'Shea, K. E. Kinetic and mechanistic evaluation of inorganic arsenic species adsorption onto humic acid grafted magnetite nanoparticles. *J. Phys. Chem. C* **2018**, ASAP, DOI: 10.1021/acs.jpcc.7b12438.
- (37) Kumar, A. A.; Som, A.; Longo, P.; Sudhakar, C.; Bhuin, R. G.; Gupta, S. S.; Anshup; Sankar, M. U.; Chaudhary, A.; Kumar, R.; Pradeep, T. Confined metastable 2-line ferrihydrite for affordable point-of-use arsenic-free drinking water. *Adv. Mater.* **2017**, *29* (7), 1604260.
- (38) Towe, K. M.; Bradley, W. F. Mineralogical constitution of colloidal "hydrous ferric oxides. *J. Colloid Interface Sci.* **1967**, *24* (3), 384.
- (39) Michel, F. M.; Ehm, L.; Antao, S. M.; Lee, P. L.; Chupas, P. J.; Liu, G.; Strongin, D. R.; Schoonen, M. A. A.; Phillips, B. L.; Parise, J. B. The structure of ferrihydrite, a nanocrystalline material. *Science* **2007**, *316* (5832), 1726.

- (40) Gout, R.; Pokrovski, G.; Schott, J.; Zwick, A. Raman spectroscopic study of arsenic speciation in aqueous solutions up to 275°C. *J. Raman Spectrosc.* **1997**, *28* (9), 725.
- (41) Yang, J.-C.; Yin, X.-B. CoFe₂O₄@MIL-100(Fe) hybrid magnetic nanoparticles exhibit fast and selective adsorption of arsenic with high adsorption capacity. *Sci. Rep.* **2017**, *7*, 40955.
- (42) Farrell, J.; Chaudhary, B. K. Understanding arsenate reaction kinetics with ferric hydroxides. *Environ. Sci. Technol.* **2013**, *47* (15), 8342.
- (43) Liu, C.-H.; Chuang, Y.-H.; Chen, T.-Y.; Tian, Y.; Li, H.; Wang, M.-K.; Zhang, W. Mechanism of arsenic adsorption on magnetite nanoparticles from water: Thermodynamic and spectroscopic studies. *Environ. Sci. Technol.* **2015**, *49* (13), 7726.
- (44) Catalano, J. G.; Zhang, Z.; Park, C.; Fenter, P.; Bedzyk, M. J. Bridging arsenate surface complexes on the hematite (012) surface. *Geochim. Cosmochim. Acta* **2007**, *71* (8), 1883.
- (45) Wagner, C. D.; Riggs, W. M.; Davis, L. E.; Moulder, J. F.; Mullenberg, G. E. *Handbook of X-ray Photoelectron Spectroscopy*; Physical Electronics Division, Perkin-Elmer Corporation: Minnesota, 1979.
- (46) Grosvenor, A. P.; Kobe, B. A.; Biesinger, M. C.; McIntyre, N. S. Investigation of multiplet splitting of Fe 2p XPS spectra and bonding in iron compounds. *Surf. Interface Anal.* **2004**, *36* (12), 1564.
- (47) Gupta, R. P.; Sen, S. K. Calculation of multiplet structure of core sp^d -vacancy levels. II. *Phys. Rev. B* **1975**, *12* (1), 15.
- (48) Beji, Z.; Sun, M.; Smiri, L. S.; Herbst, F.; Mangeney, C.; Ammar, S. Polyol synthesis of non-stoichiometric Mn-Zn ferrite nanocrystals: structural /microstructural characterization and catalytic application. *RSC Adv.* **2015**, *5* (80), 65010.
- (49) Jia, Y.; Xu, L.; Wang, X.; Demopoulos, G. P. Infrared spectroscopic and X-ray diffraction characterization of the nature of adsorbed arsenate on ferrihydrite. *Geochim. Cosmochim. Acta* **2007**, *71* (7), 1643.
- (50) Pinney, N.; Kubicki, J. D.; Middlemiss, D. S.; Grey, C. P.; Morgan, D. Density functional theory study of ferrihydrite and related Fe-oxyhydroxides. *Chem. Mater.* **2009**, *21* (24), 5727.
- (51) Hiemstra, T.; Van Riemsdijk, W. H. A surface structural model for ferrihydrite I: Sites related to primary charge, molar mass, and mass density. *Geochim. Cosmochim. Acta* **2009**, *73* (15), 4423.